Nuclear Instruments and Methods in Physics Research A 1069 (2024) 169971

Contents lists available at ScienceDirect

Nuclear Inst. and Methods in Physics Research, A

journal homepage: www.elsevier.com/locate/nima

Commissioning of the MIGDAL detector with fast neutrons at NILE/ISIS

L. Millins *, on behalf of the MIGDAL collaboration

School of Physics and Astronomy, University of Birmingham, B15 2TT, Birmingham, United Kingdom
Particle Physics Department, STFC Rutherford Appleton Laboratory, OX11 0QX, Didcot, United Kingdom

ARTICLE INFO

Keywords:
Time projection chamber
Gaseous detectors
Optical read-out

ABSTRACT

Many dark matter experiments are exploiting the Migdal effect, a rare atomic process, to improve sensitivity to low-mass (sub-GeV) WIMP-like dark matter candidates. However, this process is yet to be directly observed in nuclear scattering. The MIGDAL experiment aims to make the first unambiguous measurement of the Migdal effect in nuclear scattering. A low-pressure optical Time Projection Chamber is used to image in three-dimensions the characteristic signature of a Migdal event: an electron and a nuclear recoil track sharing a common vertex. Nuclear recoils are induced using fast neutrons from a D–D source, which scatter in the gaseous volume of the detector. The experiment is operated with 50 Torr of CF_4 using two glass GEMs for charge amplification. Both light and charge are read-out, and these measurements are combined for track reconstruction. Commissioning data has been recorded with fast neutrons at the Neutron Irradiation Laboratory for Electronics (NILE) at Rutherford Appleton Laboratory in the UK. Results of the experiment's commissioning and the performance of the detector with a high rate of highly ionising nuclear recoils are presented, along with results from low energy electrons. Initial results of light and charge read-out with low pressure noble gas mixtures are also presented.

1. The MIGDAL experiment

The Migdal In Galactic Dark mAtter expLoration (MIGDAL) experiment aims to perform the first unambiguous observation of the Migdal effect in nuclear scattering [1]. The MIGDAL experimental goal is to first measure the Migdal effect in pure CF_4 and then in mixtures of CF_4 and noble gases. The Migdal effect [2,3] occurs following a nuclear recoil due to the sudden movement of the nucleus with respect to the atomic electron cloud. The resultant excitation and subsequent de-excitation of the atom can lead, with a low probability, to the ionisation of one or more Migdal electrons, demonstrated in Fig. 1. The Migdal effect has been observed in nuclear decay [4–9], but not in nuclear scattering [10]. There is a growing interest in the Migdal effect in nuclear scattering in the direct Dark Matter (DM) community, due to the enhancement in sensitivity to low mass DM candidates thanks to additional signal from the Migdal electron [11]. As such experimental verification of the Migdal effect is of great importance to the DM community. Many experiments are already using the Migdal effect to set limits of the coupling of DM to nucleons using theory predictions [11,12].

2. The MIGDAL detector

The MIGDAL detector, described in detail in Ref. [1], is an Optical Time Projection Chamber (OTPC), shown in Fig. 2, filled with low pressure (50 Torr) CF_4. The OTPC utilises both light and charge read-out in order to perform complete 3D-reconstruction of events [13]. Moreover particle identification is provided through rate of energy loss [1]. These features enable the search for the Migdal effect signature of an electron and a nuclear recoil originating from a common vertex [1]. Charge amplification is provided by the use of two glass Gas Electron Multipliers (GEMs) [14], and charge read-out is performed using a segmented Indium Tin Oxide (ITO) anode. The charge read-out provides positional information in the x-z plane. In addition to charge, primary (S1) and secondary (S2) scintillation signals are also produced during the initial interaction, and charge amplification, respectively. Both signals are recorded using a Hamamatsu R11410 VUV photo-multiplier tube (PMT) which provides timing information and serves as the trigger for the experiment. Secondary scintillation light is also recorded using a Hamamatsu Orca Quest qCMOS camera, providing positional information in the x–y plane. The camera runs continuously in rolling shutter mode, with a maximum 9.4 MP full-frame read-out speed of 120 frames per second. Measurements presented here were recorded with a 20 ms camera exposure.

The GEMs consist of 570 μm of glass sandwiched with 2 μm of copper/nickel on either side. The GEM holes are 170 μm in diameter, with a pitch of 280 μm and the GEM forms a 10 cm x 10 cm active area,

* Correspondence to: School of Physics and Astronomy, University of Birmingham, B15 2TT, Birmingham, United Kingdom.
E-mail address: lkm892@student.bham.ac.uk.

https://doi.org/10.1016/j.nima.2024.169971
Received 30 June 2024; Received in revised form 21 September 2024; Accepted 8 October 2024
Available online 9 October 2024

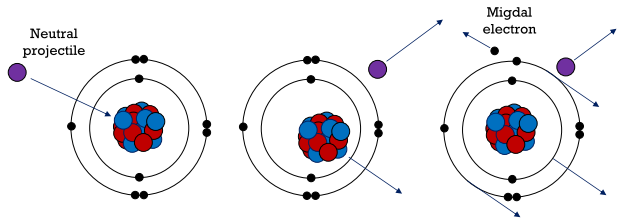

Fig. 1. Diagram of the Migdal effect following the scattering of a nucleus with a neutral projectile.

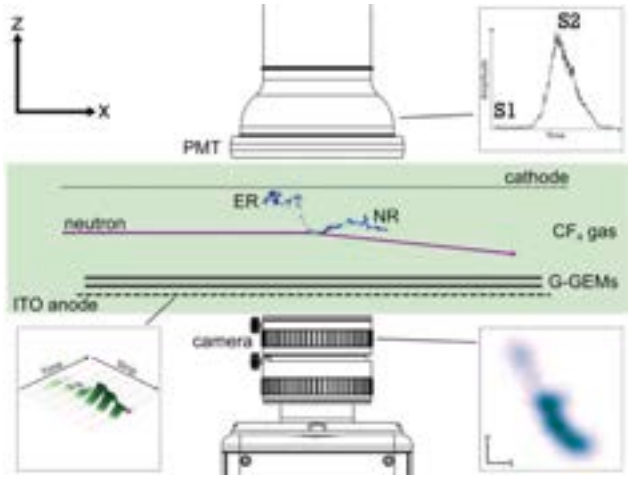

Fig. 2. A schematic of the experiment (from Ref. [1]), showing the exposure to neutrons in 50 Torr CF_4 gas, amplified using two glass GEMs with an active area of 10 cm^2 with a 3 cm drift gap. Light is read-out with a PMT and qCMOS camera, and charge is recorded by a segmented ITO anode.

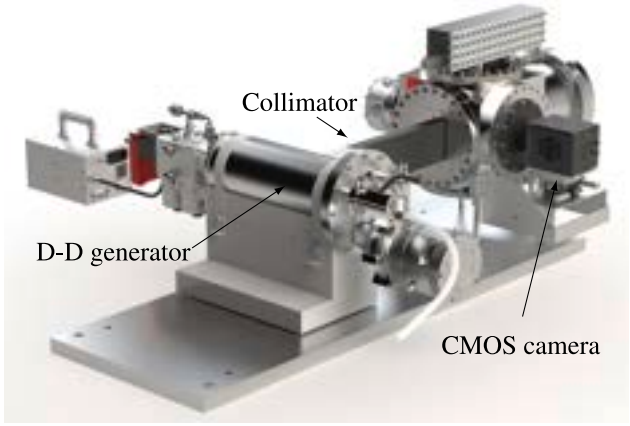

Fig. 3. The D–D generator positioned at the entrance to the collimator. The collimator is 30 cm long and is positioned at the entrance window to the detector. The detector and collimator are then surrounded by lead and BDHPE.

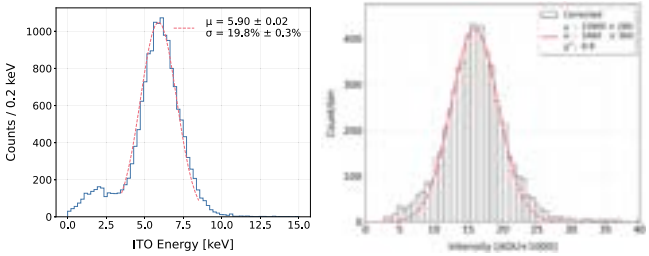

Fig. 4. ^{55}Fe spectra for the ITO (left) and the camera (right), the data are fit with a single peak Gaussian where the resolutions are found to be 20% and 22% respectively when the calibration is performed at the D–D operating gain.

with a 2 mm transfer gap between GEMs. With two GEMs the detector is operated at gains of $\mathcal{O}(10^5)$. The drift gap between the cathode and the GEMs is 3 cm. The ITO anode is segmented into 120 strips of 0.8 mm pitch read-out in pairs 60 strips apart. The ITO and PMT waveforms are digitised with a 2 ns sampling rate with 1 μs waveforms. The ITO covers the same 10 cm x 10 cm active area as the GEMs and is transparent to light, allowing light to be recorded by the CMOS camera.

Nuclear scattering is induced using neutrons from a Deuterium–Deuterium (D–D) generator at the NILE facility at ISIS, Rutherford Appleton Laboratory. The D–D generator is a source of approximately mono-energetic 2.47 MeV neutrons which are emitted isotropically with a nominal flux of 10^9 n/s.

3. Installation and calibration

The experiment was installed at the NILE facility in summer 2023, where the D–D generator was placed at the entrance to a 30 cm collimator, which is aligned to the entrance window to the detector, as shown in Fig. 3. The experiment is then surrounded by lead shielding to shield against γ-rays from processes such as inelastic scattering and radiative capture. The lead shielding is then surrounded by Borated High Density Polyethylene (BHDPE) to moderate and stop neutrons [1]. Several weeks of D–D data have been recorded, interspersed with calibration data.

The detector is calibrated using an 80 MBq ^{55}Fe source which is positioned using a remote source deployment system. ^{55}Fe calibration is regularly performed in all detector sub-systems, an example spectrum in the ITO (left) and the camera (right) is shown in Fig. 4. Calibrations are performed at the gas gains operated for D–D neutrons which requires a high dynamic range to capture high energy nuclear recoils and $\mathcal{O}(5)$ keV electrons simultaneously. At these gas gains an energy resolution of 20% is observed in the ITO, and 22% in the camera.

The calibrations of the ITO and image are shown for a data taking period in 2023 in Fig. 5, where a decrease in gain is observed during exposure to D–D neutrons. However this can be compensated for by adjusting the GEM voltages by up to 5 V daily. The cause of this decrease in gain is under investigation, however does not currently limit data taking.

4. Detector performance

4.1. Integration of subsystems

To reconstruct events in 3D, the data recorded by the ITO and PMT are synchronised with the camera images offline using timestamp information recorded by an FPGA counter. Once events are matched in time, the ITO read-out can be projected along the shared axis with the camera (x-axis), as demonstrated in Fig. 6, confirming that the events are also matched in space and the tracks have been correctly synchronised. This provides positional information in the x–y plane. The ITO read-out also provides the z-extent of the track as shown in Fig. 7 (left).

The absolute z co-ordinate is reconstructed using the time difference between the S1 and S2 scintillation signals in the PMT. The PMT is read out in two channels, a high gain channel (pink) to measure primary scintillation, and a low gain channel (blue) to measure secondary scintillation, shown in Fig. 7 (right). The time is calculated where the signal crosses 40% of the signal peak, and the time difference is combined with the drift velocity (13 $\mu m ns^{-1}$) to reconstruct the absolute depth.

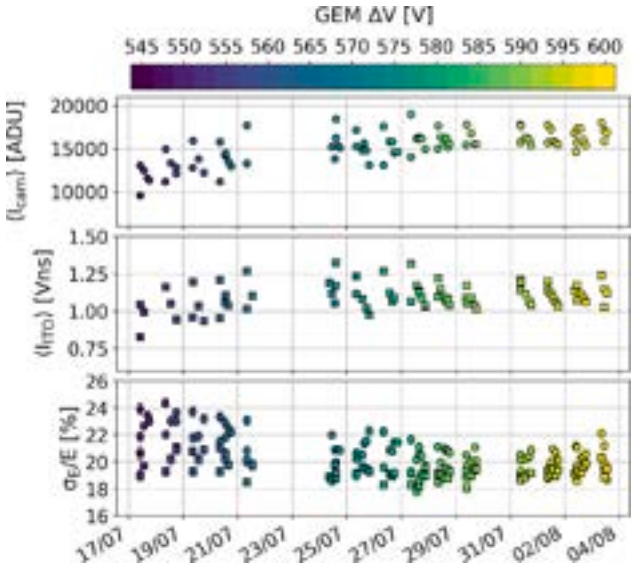

Fig. 5. ^{55}Fe calibrations over the course of a data taking period in 2023. A decrease in gain is observed during exposure to D–D neutrons which is compensated for by an up to 5 V daily increase in the GEM voltages.

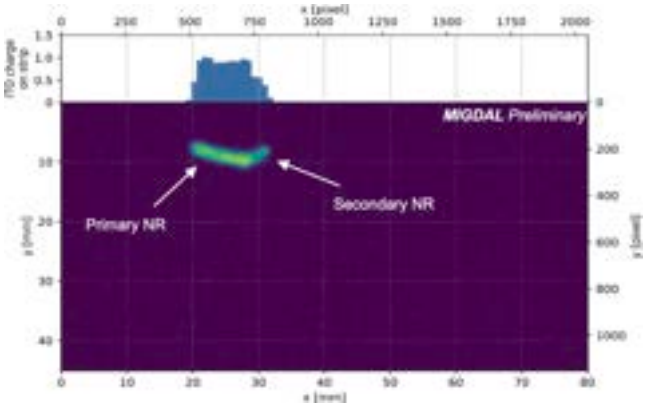

Fig. 6. An NR track with a secondary NR. The lower panel shows the image read-out, providing x–y positional information. The upper panel shows the projection of the ITO waveforms onto the shared axis with the camera, which is used to compare the image and ITO tracks to verify the track matching.

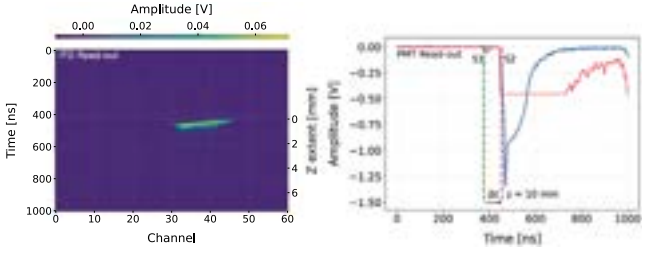

Fig. 7. (Left) ITO read-out for the track shown in Fig. 6, the channel number can be converted into a position in x, and the time over threshold is used to calculate the z-extent. (Right) PMT read-out in two channels — high gain (pink) for the primary scintillation, and low gain (blue) for secondary scintillation. The time difference between the S1 and S2 signals is used to reconstruct the absolute z co-ordinate of the interaction.

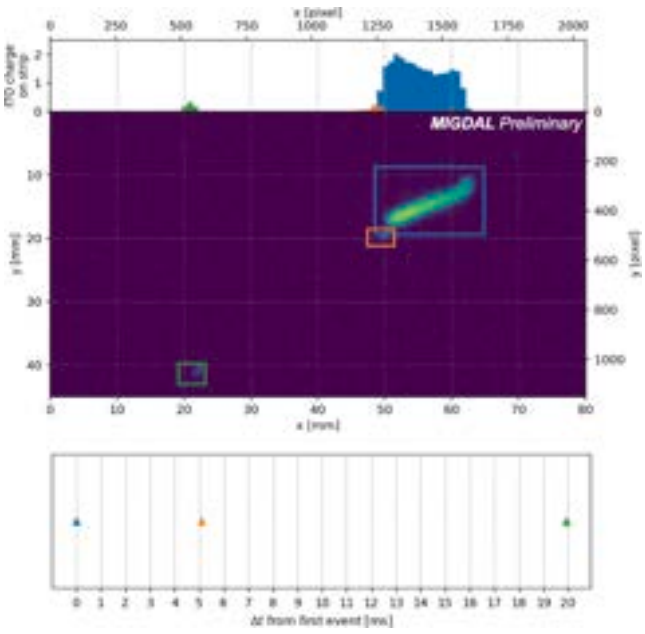

Fig. 8. 20 ms exposure image containing nuclear recoil from D–D neutrons, and electron from ^{55}Fe with the ITO projection along the top panel. A nuclear recoil track (blue bounding box) and 2 electron tracks (orange and green bounding boxes) have been identified by the YOLO object detection algorithm. Whilst this is the expected Migdal topology, the nuclear recoil (blue) and overlapping electron (orange) are clearly resolved in the ITO as separate events, with the time separation shown in the bottom panel.

4.2. D–D + ^{55}Fe results

In order to test the dynamic range of the detector, the detector was exposed to an ^{55}Fe source and D–D neutrons simultaneously, allowing nuclear recoils to be captured simultaneously with low energy electrons from ^{55}Fe. Fig. 8 shows an example event from this run containing a nuclear recoil candidate, and 2 electron candidates. Images are analysed using YOLO [15], a deep-learning based object detection algorithm, which identifies tracks in the image and draws bounding boxes, detailed in Ref. [16]. In Fig. 8, the blue bounding box shows the identified nuclear recoil candidates, and the orange and green bounding boxes show the identified electron candidates. The overlapping electron and nuclear recoil bounding boxes form the topology expected from the Migdal effect. Tracks are also analysed in the ITO, which has faster time resolution (2 ns) compared to the camera (8 ms peak). The tracks in the ITO (top panel) are shown in Fig. 8, where again the ITO is projected along the common axis with the image (middle panel). Here it can be seen that the three tracks are three separate events in the ITO, that occurred within the camera exposure. The bottom panel in Fig. 8 shows the time separation between these events, where the blue and orange markers show the time of the nuclear recoil, and overlapping electron respectively. This timing information provides powerful coincidence rejection for coincident tracks in the camera such as these.

5. Noble gas mixtures

Preliminary tests were performed with ^{55}Fe in Ar/CF_4 mixtures at various pressures. The gain curve at 60 Torr is shown in Fig. 9 for pure CF_4, and mixtures of 30%, 40%, and 50% Ar. The recorded gas gain, from the charge recorded by the ITO, is shown on the top panel, and the lower panel shows the measured energy resolution. In the Ar/CF_4 mixtures gas gains greater than 10^5 are achieved with

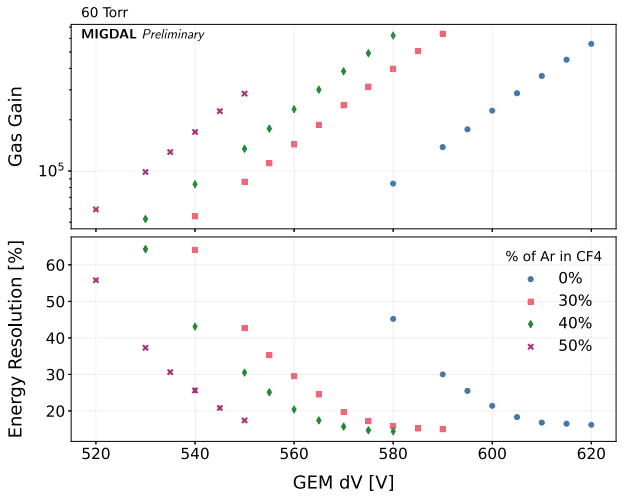

Fig. 9. Measured gas gain for Ar/CF_4 mixtures at 60 Torr for 0%, 30%, 40%, and 50% Ar in CF_4, against the potential difference across the GEMs.

lower GEM potential differences. The light output was also measured for each mixture, and an increase in scintillation light compared to ionisation charge is observed in Ar/CF_4, arising due to energy transfer between excited states of Ar and CF_4 shifting scintillation to the visible spectrum [17].

6. Conclusion

The MIGDAL experiment aims to perform the first unambiguous observation of the MIGDAL effect in nuclear scattering, first in CF_4, and then in mixtures of CF_4 and noble gases. A low pressure (50 Torr) OTPC is used to perform 3D track reconstruction. The experiment was commissioned in the NILE facility at ISIS in summer 2023, and several weeks of D–D data have been taken, interspersed with ^{55}Fe calibrations, the analysis of which is underway. The detector is able to operate with a wide dynamic range in order to image both low energy electrons and high energy nuclear recoils simultaneously. Tests were also performed in low pressure Ar/CF_4 mixtures, where an enhancement in light yield was observed with Ar.

Declaration of competing interest

The authors declare that they have no known competing financial interests or personal relationships that could have appeared to influence the work reported in this paper.

Acknowledgements

This work has been supported by the UKRI's STFC (ST/T005823/1, ST/T005882/1, ST/V001833/1, ST/V001876/1, ST/W000636/1, ST/X006042/1, ST/T000759/1, ST/W000652/1, ST/S000860/1, ST/X005976/1, ST/T505894/1, ST/X508913/1); by the U.S. Department of Energy, Office of Science, Office of High Energy Physics (DESC0022357); by the U.S. National Science Foundation (2209307); by the Portuguese Foundation for Science and Technology (PTDC/FIS-PAR/2831/2020); by the DFG, German Research Foundation under Germany's Excellence Strategy (EXC 2121 "Quantum Universe" – 3908 33306); by the Spanish Ministerio de Universidades (CA3/RSUE/2021-00827); and by the EU's Horizon 2020 research and innovation programme (841261-DarkSphere and 101026519-GaGARin). We are grateful to the Particle Physics Department at RAL and the ISIS facility for technical assistance and for hosting this experiment. For the purpose of open access, the authors have applied a Creative Commons Attribution (CC BY) license to any Author Accepted Manuscript version arising from this submission.

References

[1] H.M. Araújo, et al., The MIGDAL experiment: Measuring a rare atomic process to aid the search for dark matter, Astropart. Phys. 151 (2023) 102853.
[2] A. Migdal, Ionizatsiya atomov priyadernykh reaktsiyakh, ZhETF 9 (1939).
[3] A. Migdal, Ionization of atoms accompanying alpha- and beta-decay, J. Phys. Acad. Sci. USSR 4 (1941).
[4] F. Boehm, C.S. Wu, Internal bremsstrahlung and ionization accompanying beta decay, Phys. Rev. 93 (1954) 518–523.
[5] M.S. Rapaport, et al., K-shell electron shake-off accompanying alpha decay, Phys. Rev. C 11 (1975) 1740–1745.
[6] M.S. Rapaport, et al., L- and M-shell electron shake-off accompanying alpha decay, Phys. Rev. C 11 (1975) 1746–1754.
[7] E. Berlovich, Sov. Phys.—JETP 21 (1965) 675–680.
[8] C. Couratin, et al., First measurement of pure electron shakeoff in the β decay of trapped $^6He^+$ ions, Phys. Rev. Lett. 108 (2012) 243201.
[9] X. Fabian, et al., Electron shakeoff following the β^+ decay of $^{19}Ne^+$ and $^{35}Ar^+$ trapped ions, Phys. Rev. A 97 (2) (2018) 023402.
[10] J. Xu, et al., Search for the migdal effect in liquid xenon with keV-level nuclear recoils, Phys. Rev. D 109 (5) (2024) L051101.
[11] M. Ibe, et al., Migdal effect in dark matter direct detection experiments, JHEP 03 (2018).
[12] P. Cox, et al., Precise predictions and new insights for atomic ionization from the migdal effect, Phys. Rev. D 107 (3) (2023).
[13] E. Tilly, M. Handley, 3D track reconstruction of low-energy electrons in the MIGDAL low pressure optical time projection chamber, JINST 18 (07) (2023) C07013.
[14] H. Takahashi, et al., Development of a glass GEM, Nucl. Instrum. Methods A 724 (2013) 1–4.
[15] J. Redmon, et al., You Only Look Once: Unified, Real-Time Object Detection, 2016, pp. 779–788, http://dx.doi.org/10.1109/CVPR.2016.91.
[16] J. Schueler, et al., Transforming a rare event search into a not-so-rare event search in real-time with deep learning-based object detection, 2024, arXiv:2406.07538.
[17] P. Amedo, et al., Observation of strong wavelength-shifting in the argon-tetrafluoromethane system, 2023, arXiv:2306.09919.